

A Low Power Approach for Processing Lunar Materials

Steve Best¹, Martin E. Baltazar-Lopez², Zachary M. Burell³, Henry W. Brandhorst, Jr.⁴
Space Research Institute, Auburn University, AL 36849-5320 USA

Matthew E. Heffernan⁵ and M. Frank Rose⁶
Radiance Technologies Inc., Auburn, AL, 36849 USA

An attractive alternative method of surface blasting for excavation on the moon's surface could incorporate the use of electrically powered plasma blasting. Such a technique also allows easily adjusted explosive yield control for additional safety. This paper discusses the design, construction, and performance of a prototype plasma blasting power system and blasting probes. Electrical storage devices such as capacitors are charged slowly, and then rapidly discharged into high peak power transient loads. A Bernardes-Merryman (BM) capacitor bank configuration was used as a voltage reversal protection scheme. Tests on concrete and granite rock samples are reported. Blasting probe design effects to deliverable energy is also discussed.

Nomenclature

| | |
|-------|---|
| A | = rock factor |
| C | = capacitance |
| E | = energy |
| Q | = mass in kg of TNT equivalent explosive per hole |
| V_r | = rock volume |
| x | = fragment size |

I. Introduction

LUNAR surface applications will benefit from appropriately designed low average power consumption systems when supplied by moderate level power sources such as photovoltaic arrays or Stirling converters. For lunar resource utilization the processing of lunar materials will sometimes require high peak, low average power. The best utilization of the limited surface power resources will require the discrimination of continuous versus transient loads. The electrical power management design of high peak power transient loads will need to incorporate additional electrical storage devices such as capacitors. These storage devices will be charged slowly, and then rapidly discharged into the high power transient load. Examples of such transient loads include surface rock drilling and excavation. A complication specifically for excavation on the moon's surface is that it would be prohibitive to carry large quantities of chemical explosives to the lunar surface. The significant transportation cost and safety concerns in using payload explosives are very detrimental program issues. An attractive alternative method of surface blasting could incorporate the use of electrically powered plasma blasting. Such a technique also allows

¹ Research Engineer, Space Research Institute, 231 Leach Center, Auburn University, 36849, AIAA Member

² Research Fellow, Space Research Institute, 231 Leach Center, Auburn University, 36849, AIAA Member

³ Research Assistant, Space Research Institute, 231 Leach Center, Auburn University, 36849

⁴ Director, Space Research Institute, 231 Leach Center, Auburn University, 36849, AIAA Associate Fellow

⁵ Engineer, Radiance Technologies Inc., 231 Leach Center, Auburn University, 36849

⁶ Chief Technical Officer, Radiance Technologies Inc., 350 Wynn Drive, Huntsville, AL 35805, AIAA Associate Fellow

easily adjusted explosive yield control for additional safety. This paper will discuss the design, construction, and performance of prototype plasma blasting power system and blasting probes.

In such pulsed power systems, the operating-lifetime of the capacitors is closely dependent on the voltage reversal. One voltage reversal protection scheme commonly used with capacitor-discharging systems includes a crowbar circuit. Another reversal protection scheme used is based on a Bernardes-Merryman (BM) capacitor bank configuration. It is the nature of such a BM bank that if the system is electrically underdamped, the remaining energy will continue to move between the two capacitor banks of the BM system until equilibrium is achieved or circuit current thresholds have been reached. As a result of using this BM scheme, neither capacitor bank is ever subjected to a negative polarity voltage swing eliminating the need for crowbar circuitry. Some implementations of the BM design could easily include recovery schemes to reclaim a portion of the unused electrical energy. The BM topology was used to protect and drive our pulsed power system.

A high peak pulsed power conversion system was designed and constructed. When the discharge of energy from a reactive power storage system is under-damped, voltage and current oscillations will occur. In this system, a capacitor is charged over a long period of time at low current (power), and then discharged in a very short pulse at very high current to break blocks of concrete or large rocks. Scalable prototypes of the plasma blasting probes for electrically powered pulsed plasma rock blasting were also designed and constructed. The probe design includes a coaxial electrode assembly which is connected to the capacitor bank via a coaxial cable. The probe, along with a working fluid is inserted into a 1" diameter hole cast into concrete or drilled into granite blocks. The capacitor bank system was charged at low current, and then the bank was discharged via a switch. Peak power was measured in the megawatts. Pulse rise times were around 10 μsec and pulse lengths on the order of 200 μsec were achieved.

The blasting system is able to provide pressures well above the tensile strengths comparable to those of common rocks, i.e. granite (10-20 MPa), tuff (1-4 MPa) and concrete (7 MPa). The system was successfully tested by reducing concrete specimens into small rubble with blasting probe delivered net energy levels starting at 9 kJ and increased with capacitor bank charge voltage. Tests on concrete and granite rock test samples are reported. Blasting probe design effects on deliverable energy is also discussed.

II. Plasma blasting system

The plasma blasting system consists of the following integrated components:

A. Capacitor Bank

A Bernardes-Merryman configuration, Fig. 1, was assembled using four 206 μF capacitors with a rated voltage of 22kV and maximum peak current of 200kA each. These four high energy density capacitors are specially designed for pulsed power applications and maximum voltage reversal of 20%. Two capacitors connected in parallel and then connected in series with another set of two capacitors in parallel comprise a Bernardes-Merryman topology and are applied to produce high current pulses with no voltage reversal experienced by the capacitors. One capacitor can store 50 kJ, thus the capacitor bank could be reconfigured to provide a maximum of 200kJ.

B. Switching Device

In this prototype device an Ignitron is used to switch the high energy capacitor bank for the plasma blasting of rocks. An ignitron is a high power vacuum closing switch utilizing a pool of mercury. An igniting electrode (called the "ignitor") is briefly pulsed to create an electrically conductive mercury plasma, triggering heavy conduction between the cathode and anode. Because they are far more resistant to damage due to overcurrent or back-voltage, specially constructed pulse

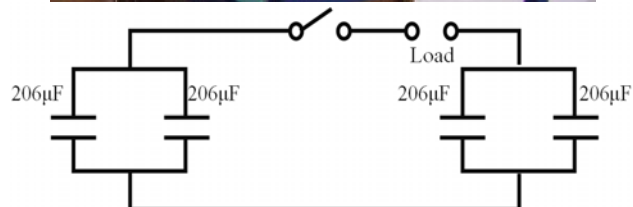


Figure 1. Capacitor bank and Bernardes-Merryman capacitor configuration.

rated ignitrons are used in pulsed power applications and usually operate at very low duty cycles. This pulsed-power class ignitron is designed to handle reverse current, with a maximum voltage of 25 kV and peak current of 600 kA. In an actual Lunar application, another type of high peak current switch would be used instead.

C. Plasma Blasting Probe

As required by the design, the probe should be scalable, safe and easy to manufacture. The design configuration, safety considerations, and choice of readily available materials were considered. The best embodiment to be used in this first prototype was a coaxial electrode blasting probe constructed by SRI's with dimensions approximately one fifth of those used by other previously reported blasting probes^{1,2}. A typical plasma blasting configuration using the Bernardes-Merryman topology is shown in Fig. 2.

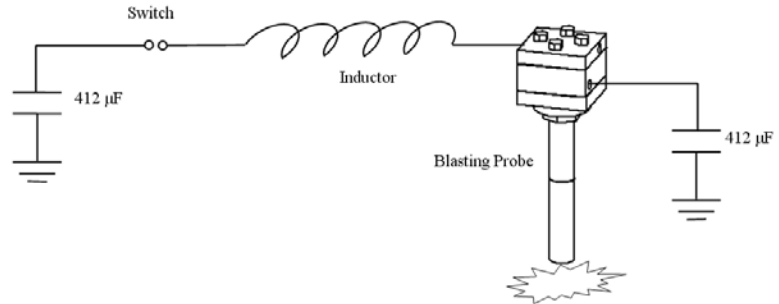


Figure 2. Typical plasma blasting system configuration

A blasting probe, Fig. 3, was constructed according to the design requirements mentioned above. The characteristics of the plasma blasting probe are:

1. Coaxial electrode configuration. This is the most practical configuration for the purpose of blasting lunar rock.
2. The external return electrode should be able to sustain the blasting force and threshold pressures as high as 2.5 GPa which can be expected when blasting, and to protect as much as possible the internal electrode and dielectric separation.
3. The connectors from the probe to the cables will be enclosed by a dielectric box or connecting box on one end of the probe.
4. The two electrodes are separated by a dielectric material assembled concentrically.
5. A recoiling device comprising four springs is integrated within the enclosing box.



Figure 3. Plasma Blasting Probe

D. Coaxial Cable

A transmission cable with the desired characteristics to support pulsed energy transfer from the capacitor bank to the blasting probe was not commercially available. Thus, a coaxial cable was constructed.

There are two issues which need attention with high voltage cable applications. The first is the level of insulation necessary to prevent arcs to adjacent components or wiring. The second is the effective diameter necessary to reduce corona losses. Reduction of corona is important because a common failure mode for insulation is the formation of small defects (i.e. pinholes) in the insulation due to corona discharges within the insulation. A breakdown test on cables assured that this effect would not be present at least up to 15 kV.

The coaxial cable, because its construction can reduce coronal discharges, thus reducing losses. Having the outer surface of the cable near ground potential initially also confers some safety advantages. It is important to note that in systems with sufficient stored energy, tens to hundreds of kJ, the coax wire can literally explode in the event of a dielectric failure. Coaxial cable also has the advantage of low series impedance in pulsed circuits and provides high strength through the high resistant mesh sleeving to resist intense forces produced by internal currents and magnetic fields.

A micro-ohmmeter was used to measure the resistance of the coaxial cable. The resistance in the center conductor was $948 \mu\Omega$, the outer braid was $1150 \mu\Omega$, thus, the pulsed power cable resistance is approximately 2.1 milliohms.

E. Ignitron trigger circuit

In order to send the short-duration energy pulses from the capacitor bank into the probe, a solid-state ignitron driver circuit and a digital delay generator (DDG) were used as the trigger circuit for the ignitron. The ignitron driver circuit has a fiber optic input triggered from the DDG. Fig. 4, shows a block schematic of the trigger circuit.

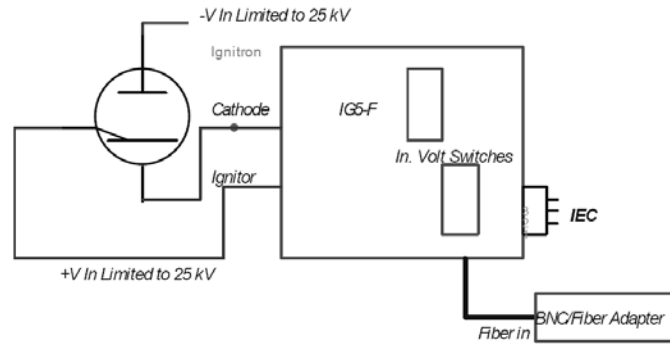


Figure 4. Schematics of the ignitron trigger circuit³.

F. Charging circuit and protective devices

In high energy pulsed power systems an isolated high-voltage capacitor-charging power supply is used to charge the capacitor bank quickly and efficiently. Capacitor-charging power supplies are a special sub-class of power supplies designed to rapidly charge large capacity bank. The power supply should be isolated and protected from the high voltage and high current driven by the capacitors bank. A typical protection circuit consists of a protection resistor in series between the capacitor-charging power supply and capacitor bank. The addition of a diode to ground incorporates some reversal protection for the power supply. An alternative to that scheme is a protection box, Fig. 5, which integrates the charging circuit and consists of two high voltage switching relays, one normally open and one normally closed, a dump resistor and a charge-interim capacitor, connected as shown in Fig. 6. In this way, unintentional reversal current goes to the charge-interim capacitor which also provides a minimal capacitive load to a capacitor-charging power supply when isolated.

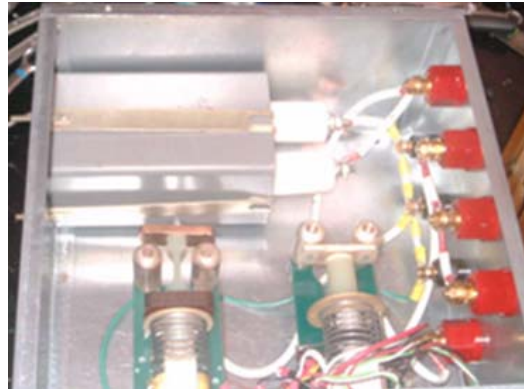


Figure 5. Charging circuit protection box.

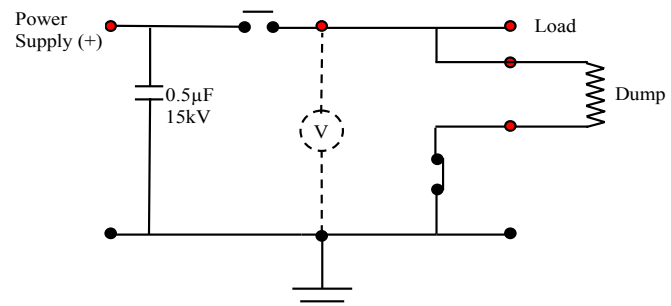


Figure 6. Schematics of a charging circuit used in a protection box.

G. High Voltage Power Supply

The backbone of the charging circuit is a capacitor charging power supply, Fig. 7. A robust high voltage capacitor charging power supply is integrated into the plasma blasting system to charge the capacitors. This is a rack-mountable high voltage power supply specifically designed for constant current capacitor charging is rated to 12 kJ/s avg. charge rate and 20kV Max. As mentioned above, capacitor-charging power supplies charge the large capacity bank quickly to minimize the time that capacitors and switches are under high voltage stress.

The power supply is connected to the capacitor bank through the charging circuit to isolate it from the capacitor bank during the discharge and to protect from current reversal.



Figure 7. High voltage power supply.

H. Diagnostics subsystem

The diagnostics subsystem, Fig. 8, was integrated by four high voltage probes, one current monitor (Pearson coil) and an oscilloscope. The low bandwidth, high voltage probe connected to a digital voltmeter is a 1000:1 voltage divider formed by two matched metal-film resistors for measurements up to 40kV. This probe was used to monitor the charging voltage from the power supply at the charging circuit box.

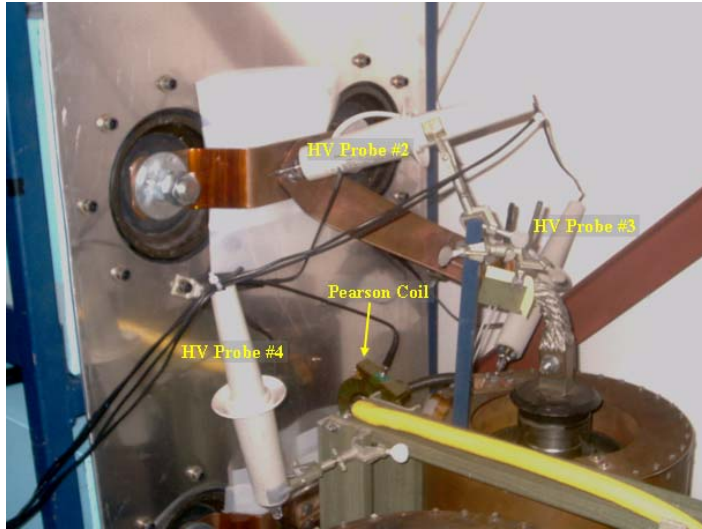


Figure 8. Location of diagnostic devices.

For monitoring the current, a Pearson coil was installed around the ignitron anode lead. The three high voltage probes and the Pearson Coil, are connected to a four channel oscilloscope.

The remaining three high voltage probes with a capacity of 20 kV DC/40 kV peak (100 ms pulse width) were used for measurements of voltages at several points after the capacitors. The 75 MHz bandwidth of those probes enables the capture of fast, high-voltage signals. In one configuration, one of the probes was connected to the capacitor bank; a second probe was attached to the ignitron cathode and the third one on the second capacitor bank of the B-M topology. In a later configuration, the latter two probes were differentially connected to either side of the blasting probe with their ground leads connected to each other.

III. Plasma blasting of concrete cylinders

Before actually breaking large granite rocks, it was necessary to characterize the plasma blasting system. We started testing the system by breaking small concrete cylindrical blocks of 12in diameter by using a charging voltage of 9 kV, Fig. 9. Then bigger cylindrical blocks of 18 in diameter were blasted using a charging voltage of 11kV, Fig. 10.

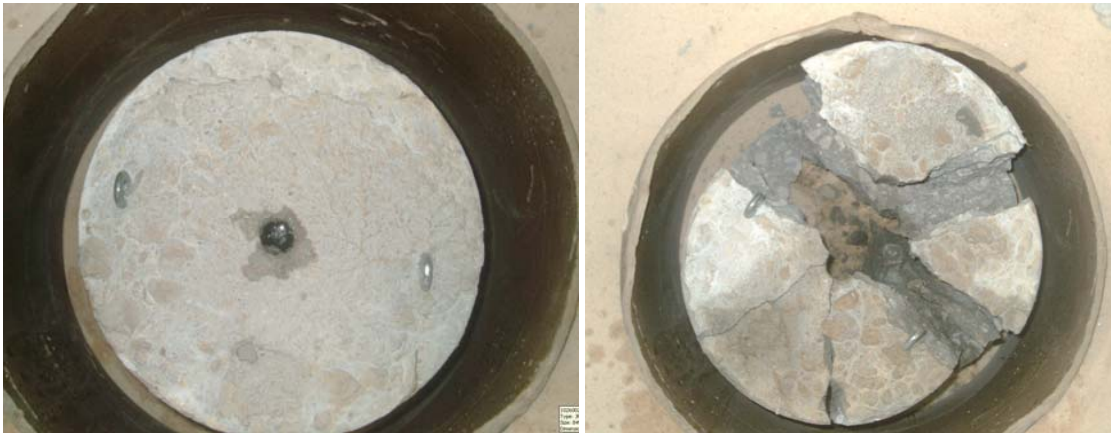


Figure 9. Concrete specimen, 0.022m³ (0.785 ft³), before and after blasting with charging voltage of 9kV.

For mining on the Moon's surface, the plasma blaster system should be capable of bursting not only rocks but soil. To this regard, the lunar soil can be emulated as a semi-infinite body, where a certain volume of material is always confined in all directions except at the surface, where spalling is expected with blasting. When the plasma blaster is operated with the blasting probe, the following sequence of events occurs: The high temperature plasma vaporizes a working fluid (in this case water), reaching temperatures of about 3000 to 4000 °C, which is confined in the blaster probe cavity and will not be able to dissipate, thus pressure is formed. As a result, a blast wave – a layer of compressed water vapor – is formed in front of that vapor containing most of the energy. The major cause of all the destruction is the impact of this wavefront. This blast wave starts propagating out toward regions with lower

pressure, i.e., atmospheric pressure. As the wave propagates, the pressure of the blast wavefront falls with increasing distance. This finally leads to cooling of the gases and a reversal of flow as a low-pressure region is created behind the front resulting in equilibrium. When that pressure, which could reach up to 2.5GPa, exceeds the tensile strength of the concrete, which is roughly one tenth of the compressive strength, fracture is expected. Thus the blasting ability would be dependent on the strength of the concrete and any reinforcement around the hole in which the plasma blaster probe is placed. In this case the concrete used was normal-strength concrete with 4700psi compressive strength.

A. Energy fed into the blasting probe

In the initial configuration of the voltage probes, the exact amount of energy put into the plasma blasting probe could not be determined due to limitations on diagnostic devices and inherent losses of energy at the ignitron, the transmission cable and connections. However an approximation of the energy spent in the cable along the plasma blasting probe was obtained from Joule's Law applied to the waveforms.

For each of the tests, the energy waveforms were processed by subtracting the waveform voltage left at capacitor bank No.2 from the waveform voltage at ignitron's cathode. Then the voltage waveform from the difference was multiplied times the current, giving a power waveform. Finally, the power waveform was integrated with respect to time to obtain energy.

Later in the test series, two of the high voltage probes were relocated near the blasting probe and connected differentially. This scheme allowed for more accurate measurement of the voltage drop across the blasting probe. This in turn produced more accurate power and energy measurements.

Also the energy content at each stage of the experiment, where it was possible to have a diagnostic device, was performed. The energy left on the capacitors banks in a B-M configuration was calculated directly from the squared voltage waveforms of the voltages at capacitor bank No.1 and capacitor bank No.2 respectively. The energy on each capacitor bank was obtained and the energy spent at the blasting probe calculated. Samples waveforms and energy analysis plots are shown in the Appendix.

IV. Granite rock test.

Using the same probe, electrode gap, and charge voltage, a granite rock of approx. 0.085 m^3 (3 ft^3), Fig. 11, was tested next. A hole was drilled on one of the flat surfaces of the rock up to a depth of six inches, corresponding to the same depth of the concrete blocks previously broken. Like the concrete cylinders, the rock was tested by holding the blasting probe through the mounting bridge with a chain as shown in Fig. 11. The result of this test was the granite rock broken in 6+ pieces, Fig. 12.



Figure 10. Concrete Sample, 0.075 m^3 (2.65 ft^3), after blast with a charging voltage of 11 kV.



Figure 11. Granite rock, approx 0.085 m^3 (3 ft^3) ready to be blasted.



Figure 12. Granite rock after plasma blasting.

The energy of the blast can be related to the amount of damage by measuring the new surface area created by the blast. In this case, the new area resulted proportional to the energy used, the more energy used, the more the damage and then the more new surface area produced by the blast.

The energy waveforms were processed by subtracting the capacitor bank #2 voltage waveform from the ignitron's cathode voltage waveform, which is the voltage difference between the coaxial cable and blasting probe. Then the voltage difference waveform multiplied by the current waveform yields a power waveform. Finally, the power waveform was integrated respect to time to obtain energy.

A. Electrode gap and energy delivered relationship

In an attempt to find a relationship between electrode gap and current level, and consequently in the amount of energy sent into the blasting probe to break the specimen, the electrode gap was systematically increased. In doing so, it was expected that the resistance between electrodes should increase, thus changing the current for the same amount of voltage. The electrode gap was varied among different tests from 0.2" to 1" to measure the effect on the resistance, current, and power.

As can be observed in Table I, there were several modifications to the blasting probe, and the electrode gap was increased as part of the modifications of probe No.1.

Given the limited number of test samples along with other factors such as changes in the probe and the way concrete samples were prepared, the correlation between parameters has not always been obvious. However, the tests have provided an approximation of such relationships.

Larger concrete specimens, of the order of 0.18m³ (6.3 ft³) were tested and the pulsed energy was doubled by increasing the charging voltage up to 16 kV. Furthermore a longer blasting probe, 12", was built for use with bigger specimens, thus facilitating the fracture of those specimens. Some other tests included pre-cracked granite rocks, in which, due to drainage, it was necessary to use gelatin instead of water in the blasting hole to successfully break the rocks.

V. Determination of Volume to be blasted

At this point, we roughly know how much energy is spent during blasting. This value of energy can be compared to the equivalent energy from a chemical explosive. This is important because most of the literature for calculating parameters of blasting is related to chemical explosives. In addition, it would be useful to correlate the energy used in the blast to a specific volume of rock or concrete to be broken.

Other approaches, like dynamic fracture mechanics, have been used to obtain a quantitative fragmentation for some blasting conditions⁴ and characterization of fragmentation mechanisms due to explosive loading. Other approaches combine fracture mechanics with finite element method^{5,6} to simulate the fracture phenomena due to blasting. Blasting is often referred to as an "art", and most progress in efficient blasting has been made by empirical observations by miners and blasters with field

Table I. Probe characteristics and related energy.

| Shot No. | Probe Length (inches) | Electrode gap (inches) | Energy spent at Probe and cable (Joules) |
|----------|-----------------------|--------------------------|--|
| 11 | 5.5 | 0.22 | 313 |
| 12 | 5.5 | 0.22 | 271 |
| 13 | 5.5 | 0.22 | 2535 |
| 14 | 5.5 | 0.22 | 2028 |
| 15 | 5.5 | 0.22 | 1647 |
| 16 | 5.5 | 0.2 | 9164 |
| 17 | 5.5 | 0.2 | 10713 |
| 18 | 5.5 | 0.2 | 9105 |
| 19 | 5.5 | 0.2 | 11348 |
| 20 | 5.5 | 0.2 | 9353 |
| 21 | 4.5 | 0.28 | 11390 |
| 22 | 4.5 | 0.28 | 12,424 |
| 23 | 4.5 | 0.28 | 13,742 |
| 24 | 4.5 | 0.55 | 16,587 |
| 25 | 4.5 | 0.55 | 15935 |
| 26 | 4 | 0.8 | 12840 |
| 27 | 6 | 0.186 (Lateral blast) | 11258 |
| 28 | 12 | 1 | n/a |
| 29 | 12 | 1 | 3697 |
| 30 | 12 | 1 | 3551 |
| 31 | 6 | 0.5 (Lateral "V" gap) | 9523 |
| 32 | 6 | 1 | 5344 |
| 33 | 6 | 1 | 9367 |
| 34 | 6 | 1 | 5344 |
| 35 | 6 | 1 | 2677 |
| 36 | 6 | 1 | 26834 |
| 37 | 6 | 1 | 38232 |
| 38 | 6 | 1 | 17763 |
| 39 | 12 | 1 | n/a |
| 40 | 12 | 1 | 37180 |
| 41 | 12 | 1 | 27694 |
| 42 | 6 | 1 | 20929 |
| 43 | 12 | 1 | 23068 |
| 44 | 12 | 1 | 23633 |
| 45 | 6 | 1 | 27123 |

experience. Here we estimate the volume of material to be broken corresponding to the energy spent in the blast and a hydrocode model is used to simulate the damage.

B. Kuznetsov equation

There are some empirical methods for the design and calculation of blasting with explosives used by the mining industry, which are available via the explosives manufacturers. However, most of those calculations are based on specific sizes of bench mining with multiple blasting holes and could not be adopted for specimens with a single-blasting hole. There is a model which relates the size of the broken fragment with the rock volume broken and the mass of equivalent explosive that could be used to predict the breakage on our specimens, developed by Kuznetsov^{7,8}. The discrepancies that can occur are due to possible energy loss during blasting.

We use the Kuznetsov equation relating the equivalent mass of TNT needed to blast a given volume of rock,

$$\bar{x} = A \left(\frac{V_r}{Q} \right)^{0.8} Q^{1/6} \quad (1)$$

where the rock factor A=7 for medium rocks, 10 for hard, high fissured rocks, 13 for hard weakly fissured rocks.

In this case we use the energy from equivalent chemical explosive mass corresponding to the spent energy at the blasting probe according to Table II.

Table II. Equivalent mass of chemical explosive

| Energy Spent in probe and cable (kJ) | Equivalent mass (for energy content) of TNT (gr) |
|---|---|
| for 11kV charge | 9 |
| for 11kV charge | 12 |
| for 16kV charge | 17.7 |
| for 16kV charge | 26.83 |
| for 16kV charge | 29.99 |
| for 16kV charge | 37.2 |
| for 16kV charge | 38.23 |

Once the equivalent mass for energy content of chemical explosive (TNT) is calculated for each energy level (energy spent on probe and cable), the Kuznetsov equation is applied, taking average fragment sizes from 1 to 40cm, and a Rock factor of A=10. The volume is found for each corresponding average fragment size and then plotted as in Fig. 13. The broken rock volume was obtained for several energy levels corresponding to energy spent on the probe and cable for different cases. Because most of the calculated energy spent in probe and cable for charging voltages of 11 kV were between 9 and 12 kJ, those values were taken as reference. On the other hand, for 16kV charging voltage, the variation on calculated energies was greater, thus more energy values were taken as reference for volume of broken rock estimation.

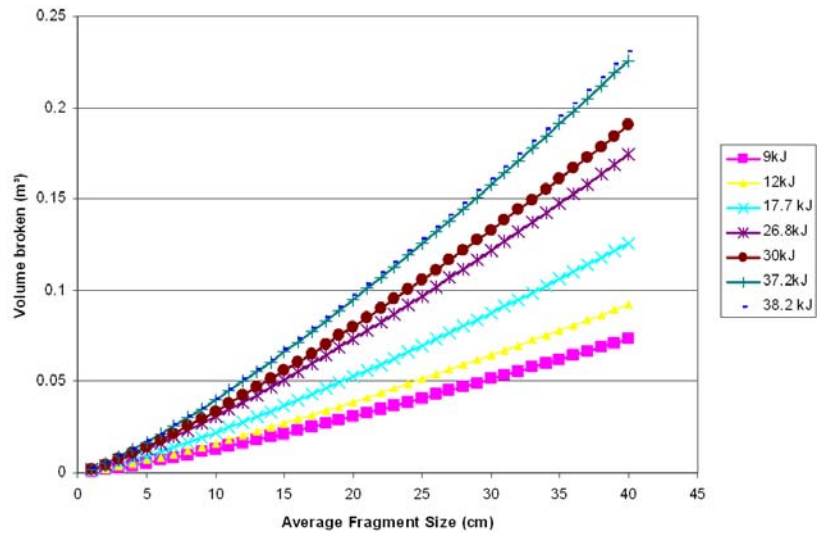


Figure 13. Adaptation of Kuznetsov equation for Rock volume broken at different energy levels.

C. Prediction of Volume to be fractured

These first series of tests were aiming to establish a relationship between energy used as a function of rock fracture. Also, according to the results from Noranda-Maxwell experiments obtained by Pronko, et al.⁹, when the Plasma Blasting Technique is applied to fracture concrete blocks, there is a linear relationship between the volume of material to be fractured with respect to the energy used. Those experiments were carried out at energy levels between 300 and 1000 kJ. Based on this linear trend, a prediction was made on the volume of material to be fractured, Fig. 14. By applying the same linear trend at lower energy levels, below 60 kJ, the energy used was extrapolated and then compared to the real energy expenditure to fracture samples of different volumes.

As it can be observed, in Fig. 15, there is a considerable deviation on the trend line of the real actual energy used respect to the predicted with the linear trend. As the energy and volume is increased, the deviation is also augmented. The maximum difference was 34% between predicted and actual energy for a concrete sample of 0.34m³. There are two possible explanations to that deviation. First, it could be possible that the Noranda-Maxwell linear trend which was obtained for higher energy values, 300 to 1000 kJ, may be no longer valid for our lower energy levels or secondly, the plasma blaster system described here is more efficient at low energy levels. To this regard more experimentation is needed.

D. Hydro-code simulations

Simulations of the blasting were performed using a hydrocode. The concrete was modeled using a porous EOS and a Drucker-Prager strength model. Values of the Bulk modulus E , and the ultimate compressive strength f_c were obtained from bench tests. Here we present some results of preliminary attempts to model electro-hydraulic loading on concrete cylinders. All simulations were performed using 2-D axial symmetry, a computationally efficient way to simulate the loading of a 3-D cylinder. In parallel with our experimental work, we modeled cylinders having dimensions of 12" diameter X 12" high, and 18" diameter X 18" high.

The potential utility of hydro-codes is that they could provide means to investigate explosive loading without actually having to perform as many large, expensive experiments. However, the use of hydro-codes must first be justified by the convergence of numerical and experimental results. Therefore in this paper we also present preliminary results that demonstrate such convergence for blasts performed on 12" and 18" cylinders.

There are 2 basic loads applied to the concrete during electro-hydraulic blasting. There is the initial shock wave blast on the inside of the borehole which initiates cracking in the sample. This is followed by a slower loading phase from the expanding hot gases which penetrate and evolve the cracks initiated during shock wave loading. In the simulations we report here we only investigate the shock wave loading due to stress exerted inside the borehole in order to understand how loading rates determine the initial cracking pattern. The expanding gases only magnify the initial cracks, and thus an improved understanding of the initial cracking should improve overall blast efficiency.

We simulated the blast loading by applying stress boundary conditions to the borehole faces. This approximates the loading experienced in a real cylinder with a blast probe electrode gap of 1". The loading rate was estimated from I-V traces obtained during actual testing. This is not unreasonable considering that energy is being delivered to the water precisely when the current flowing through it is a non-zero value. In our simulations we include two different loading rates, each of them having the same profile, but differing in magnitude and duration. Loading

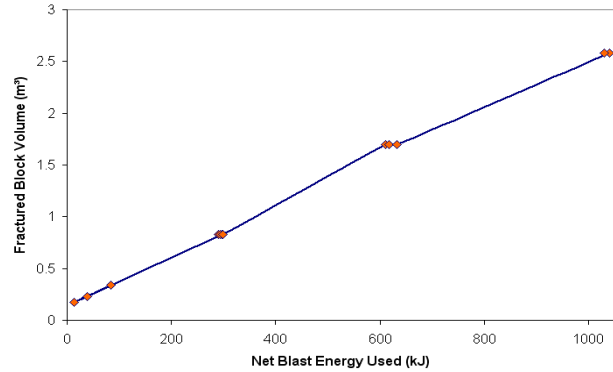


Figure 14. Volume of rock fracture as a function of net blast energy.

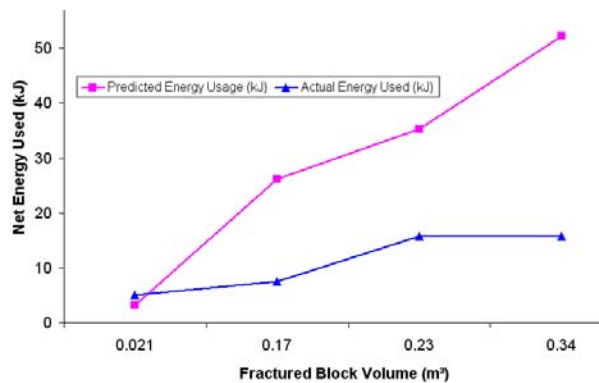


Figure 15. Comparison of Predicted vs. Actual Energy levels to fracture concrete blocks

magnitudes were estimated as described by Wakeland et al.¹⁰, and load profiles had the form of an underdamped harmonic oscillator.

Two loading rates were evaluated and are plotted in Fig. 16. The results from simulation and comparison with a blasted sample are shown in Fig. 17. As it can be observed, the numerical model utilized in simulations can be validated since the numerical results are comparable to the experimental ones. Note that in the simulation the damage (cracks) extends to an inner portion of the specimen, meanwhile in the experiment, the crack propagated all the way out to the external walls. This is due to the fact that the simulation did not take into account the effect of the expanding gases following the early shock wave.

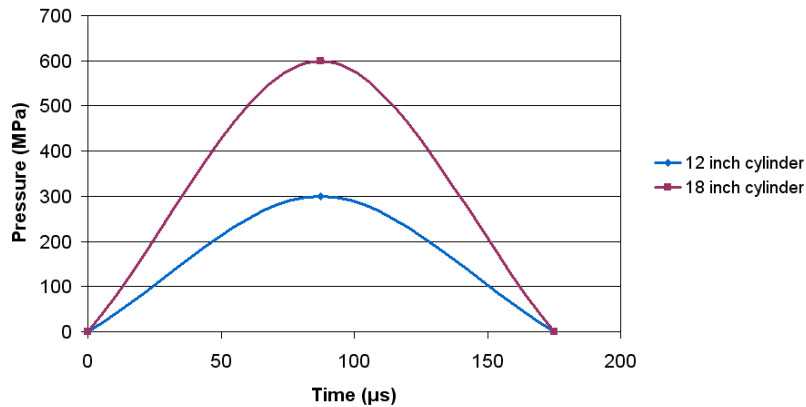


Figure 16. Examples of loading rates used in simulation

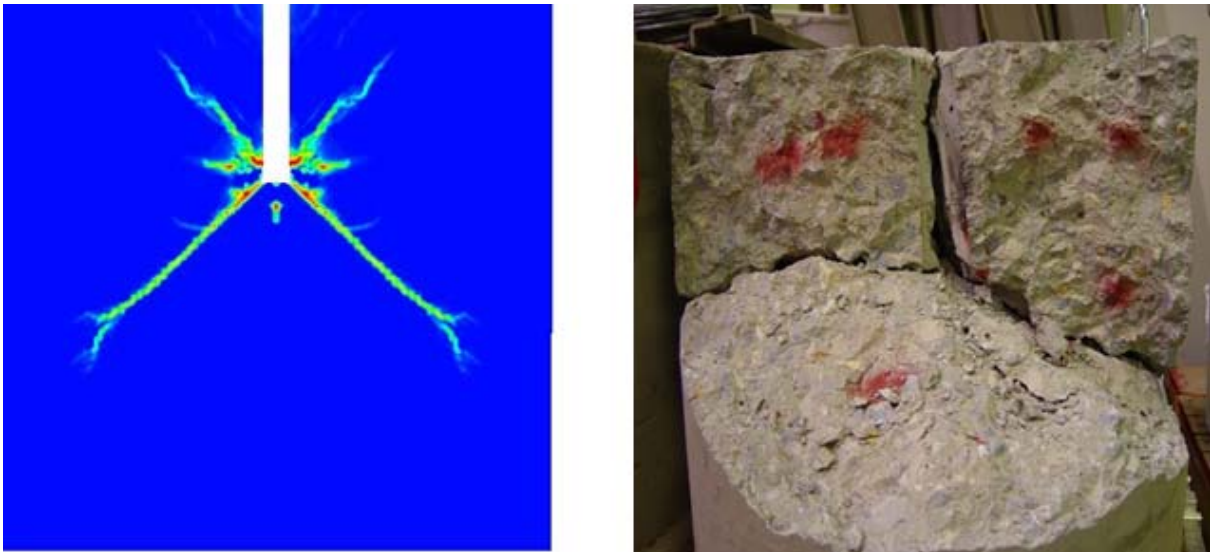


Figure 17. Simulated Damage and concrete specimen after blast, 18 inch cylinders, 0.075m³ (2.65 ft³). Loading deposition time:175μs.

VI. Conclusion

The integration of components for a first prototype of plasma blasting system for mining on the Moon's surface was carried out including a construction of plasma blasting probe, pulsed cable and charging protection box. The plasma blasting system was used to break concrete specimens and granite rocks. Blasting tests were successfully performed at several energy levels. An approximate correlation of electrode gap distances to energy levels in the blasting probe was determined. Analysis of discharge waveforms was carried out and the energy was determined at each stage of the system to estimate the total energy delivered to the probe. The volume of broken rock for different energy levels and damage was estimated.

VII. Acknowledgements

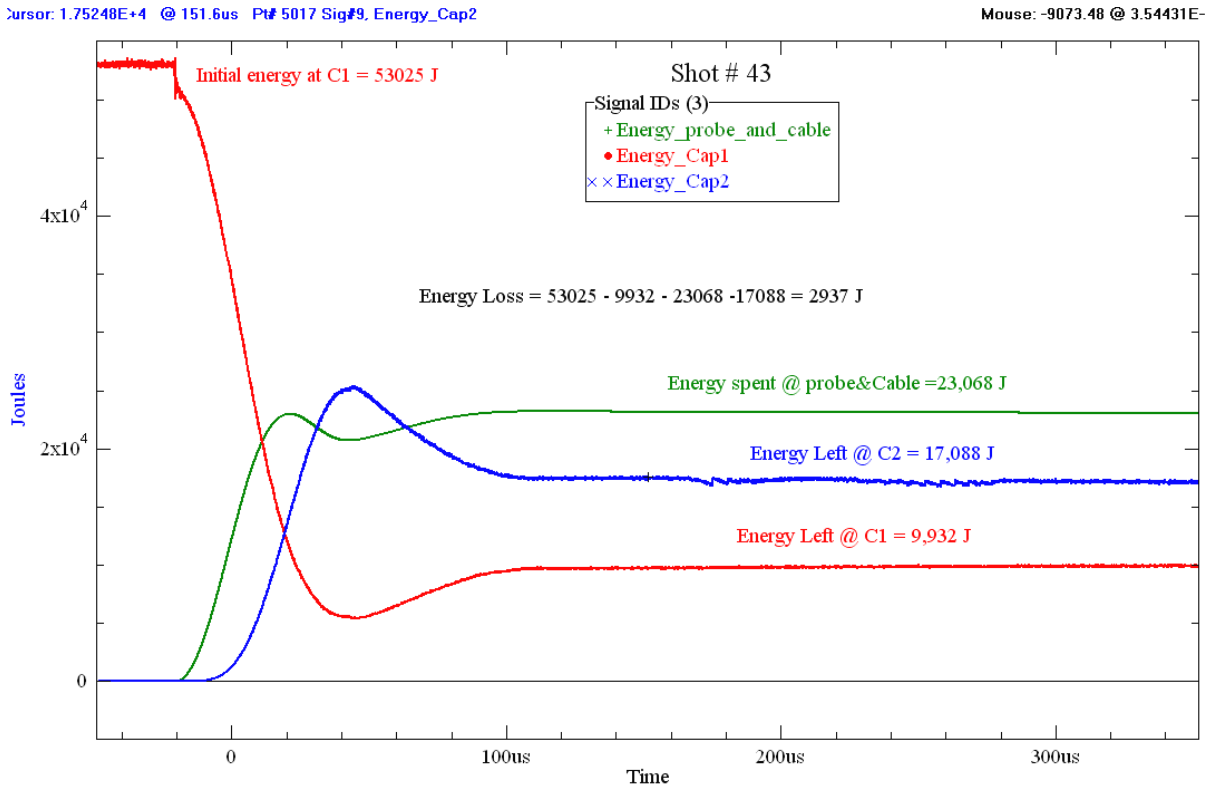
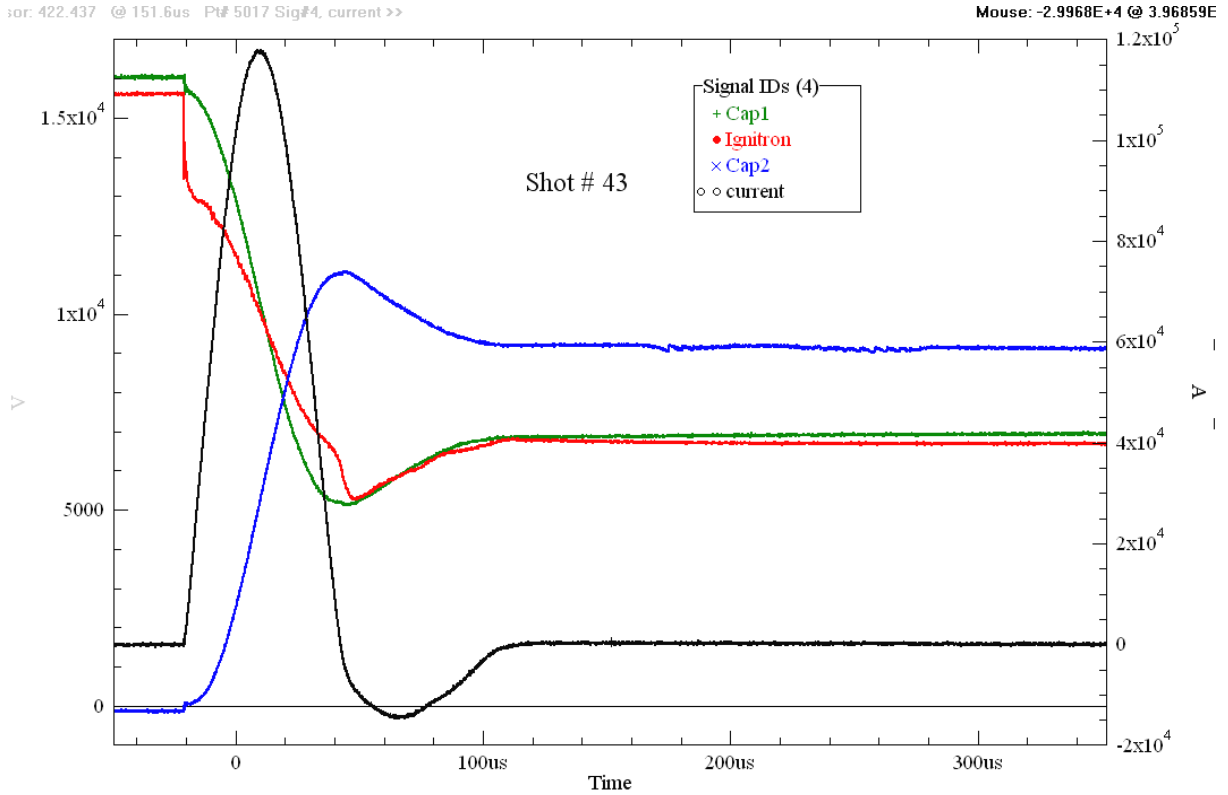
This work was supported under NASA Contract No. 07-060287 , “Highly Efficient High Peak Power Electrical Systems for Space Applications” funded through Radiance Technologies, Inc.

Any opinions expressed are those of the authors and do not necessarily reflect the views of NASA.

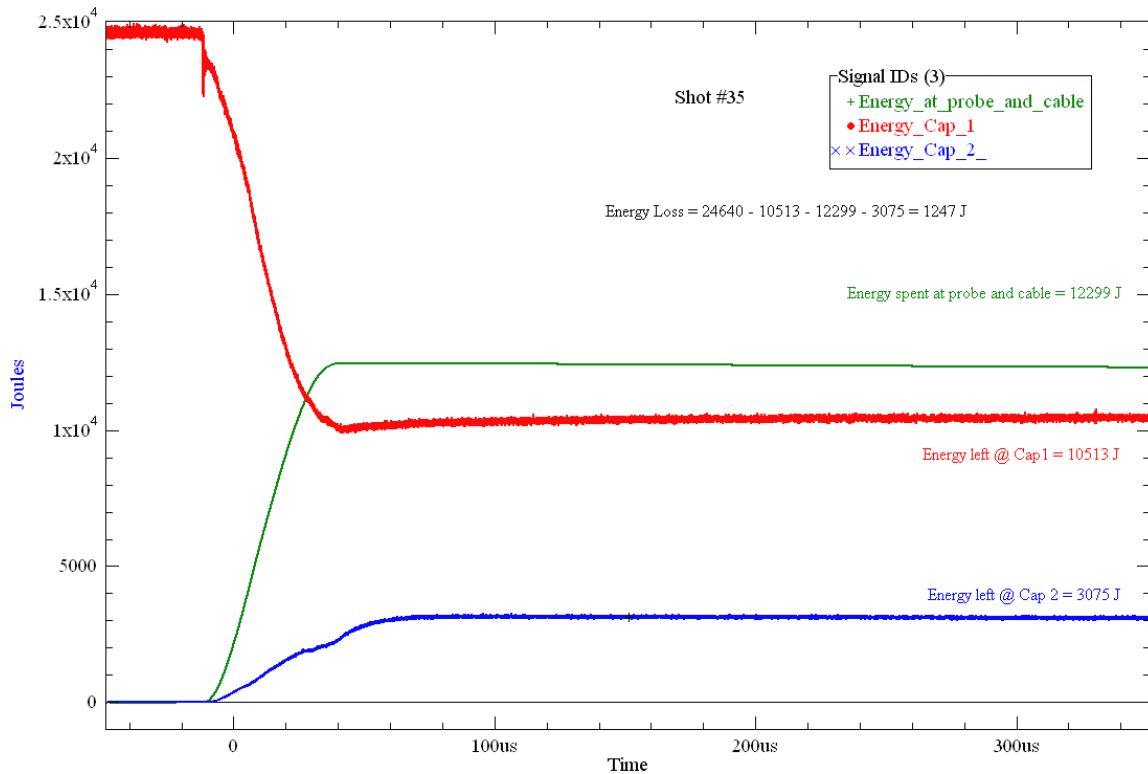
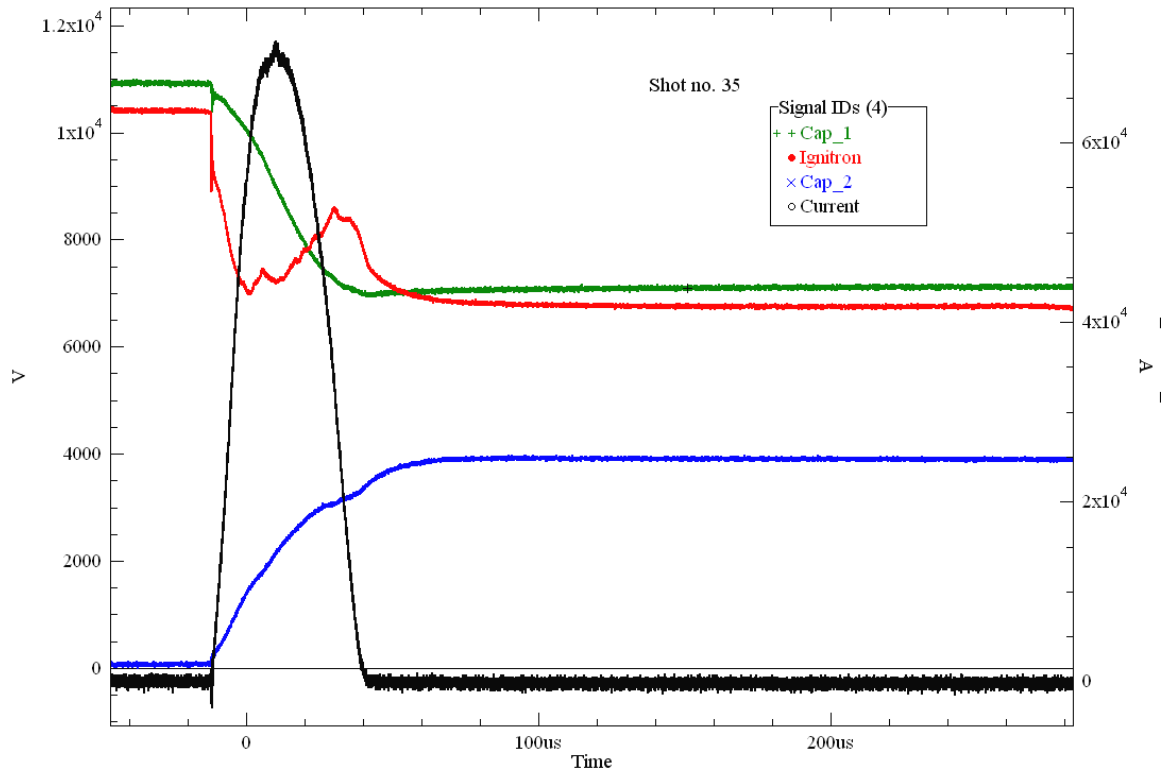
VIII. References

1. Wint G., Menard M., U.S. Patent No. 5482357 “Plasma Blasting probe assembly”, Jan 9, 1996.
2. Kitzinger F., Nantel J., U.S. Patent No. 5106164 “Plasma Blasting method”, Apr 21, 1992.
3. Northstar Research Co., Northstar High Voltage, IG5-F2 Ignitron driver Manual, 2004.
4. Rossmannith H.P., Daehnke A., Knasmillner R.E., Kouzniak N., Ohtsu M. And Uenishi K., Fracture Mechanics Applications to Drilling and Blasting, Fatigue Fract. Engng Muter. Struct. Vol. 20, No. 11, pp. 1617-1636, 1997.
5. Preece, D. S., Blasting Induced Rock Fragmentation Prediction Using the RHT Constitutive Model for Brittle Materials Proceedings of the Annual Conference on Explosives and Blasting Technique, CONF 29; VOL 2, pages 375-382, 2003.
6. Chung S. H., Preece D.S., Explosive Energy and Muck-Pile Diggability, International Society of Explosives Engineers 1999G Volume 2 - P 241, 2000.
7. Kuznetsov V. M., The mean diameter of the fragments formed by blasting rock, Journal of Mining Science (Soviet Mining science), Vol.9 No. 2, 144-148, 1973.
8. Chung S.H.; Katsabanis P.D., Fragmentation prediction using improved engineering formulae, Fragblast, Vol 4, Numbers 3-4, 198-207(10), 2000.
9. Pronko,S. et al. "Megajoule Pulsed Power Experiments for Plasma Blasting Mining Applications". in Proceeding of the 9th IEEE Pulsed Power Conference, Albuquerque, June 1993.
10. Wakeland P., Kincy M., Garde J., Hydrodynamic Loading of structural components due to electrical discharge in fluids, 14th IEEE International Pulsed Power Conference, 2003. PPC-2003. Vol 2, Issue 15-18 June, pp 925-928, 2003.

Appendix. Waveforms and energy plots for sample test shots.



Waveform and energy analysis for test shot No. 43, Approx. 0.34m³ concrete sample.



Waveform and energy analysis for test shot No. 35, Approx. 3 ft³ Granite Rock.